



## Stabilizing Co, Ni and Cu on the h-BN surface: Using O—O bond activation to probe their performance as single atom catalyst

Jagannath Datta <sup>a</sup>, Chiranjib Majumder <sup>b,\*</sup>

<sup>a</sup> Analytical Chemistry Division, Bhabha Atomic Research Centre, Variable Energy Cyclotron Centre, Kolkata, 700064, India

<sup>b</sup> Homi Bhabha national Institute, Chemistry Division, Bhabha Atomic Research Centre, Trombay, Mumbai, 400085, India



### ARTICLE INFO

#### Keywords:

Single atom catalysis  
Hexagonal boron nitride  
Vacancy defect  
Density functional theory

### ABSTRACT

The stability of isolated metal atom on a support plays very crucial role to avoid ensemble effects of agglomeration and clustering. Defects in support matrix provide additional binding to enhance the stability of single atom catalyst. Here, using plane wave based pseudo-potential approach, we report the activation of oxygen molecule by Co, Ni and Cu embedded h-BN sheet with both B and N vacancy. We have used O—O bond stretching as probe for the activation. The results show that the stability of these metal atoms is higher at the vacancy site than on pristine h-BN. The atomic charge distribution of the metal embedded h-BN sheet suggests that while for boron vacancy defects metal atoms donate electronic charge, for nitrogen vacancy defects metal atoms accept electronic charge from the sheet. The chemical reactivity of the M doped h-BN sheet has been analyzed through electronic density of states spectrum. The interaction of O<sub>2</sub> molecule with metal supported h-BN sheet suggests that the interaction energy as well as the O—O bond stretching is higher on metal atom at the nitrogen defected site. A case study of CO oxidation on the Cu embedded N<sup>V</sup> sheet has been demonstrated by co-adsorption of CO and O<sub>2</sub> molecules.

### 1. Introduction

Hexagonal boron nitride (h-BN) is a large gap insulator despite being iso-electronic and iso-structural with graphene. Because of the dielectric property of the h-BN, it is often used as the support for epitaxial growth of graphene. In terms of its physico-chemical properties, the free standing h-BN monolayer is an electrical insulator and chemically inert to oxidation and reduction. However, the chemical reactivity can be induced in the h-BN sheet by creating asymmetric charge and spin distribution [1]. Unlike graphene, the h-BN consists of hetero-atomic bonds between B and N. Thus it is possible to generate different nature of vacancy sites unlike the case of iso-electronic graphene. In this context a large number of theoretical calculations have been carried out to understand the atomic, electronic and magnetic properties of defects in hexagonal boron nitride [2–5]. One of the ways to create such asymmetry in h-BN is by creating B-vacancy or N-vacancy in h-BN sheets. In recent times, a plethora of research activities in heterogeneous catalysis have emerged based on single atom catalysis because of its higher activity and selectivity [6–8]. Nowadays, experimental research on single atom catalyst became feasible because of the advancement in technological tools [9,10]. On the basis of the reported studies it is found that in

case of SAC, the active metal atoms are dispersed on supports like metal oxides (FeO<sub>x</sub>, TiO<sub>2</sub>, CeO<sub>2</sub> etc) or N doped nanotube/carbon materials [11,12]. Few studies are also reported on the h-BN support [1,8]. One of the major challenges of SAC is the stability of isolated metal atoms (high surface energy) at reaction conditions. There is a high probability that under finite temperature the metal atoms will diffuse and form small clusters, consisting of 9–10 atoms or even nanoparticles (~1 nm). In this context we may recall that the electronic properties of a surface varies with its morphology or in other words the chemical reactivity of a surface is higher at the defects like vacancy, kinks, steps etc. From the previous studies it has been found that the metal atoms can bind at the vacancy sites much stronger, which will hinder the sintering process drastically.

Two dimensional BN (h-BN) shows higher thermal conductivity and thermal stability than graphene [13–16]. There are numerous computational studies performed to explore the suitable SACs for different purposes, e.g., (i) towards CO oxidation [8,17–19], (ii) hydrogenations of nitro-aromatic reaction on immobilized Pd nano-particle [20], (iii) effective aerobic oxidative cross-esterification of alcohols over Au/porous boron nitride catalyst [21], (iv) nitrogen fixation based on a defective BN monolayer [22], where embedded metal atom acts as

\* Corresponding author.

E-mail address: [chimaju@barc.gov.in](mailto:chimaju@barc.gov.in) (C. Majumder).

active centre of the above reactions. The oxygen reduction reaction (ORR) using pristine and defected h-BN sheets supported on Ni, Cu, Ag, Pd, and Pt were also reported [1,6,23,24]. These results help to conclude that the CO oxidative reaction in presence of O<sub>2</sub> molecule over metal doped defected h-BN support. For oxidative chemical reaction, the activation of O—O bond acts as the rate limiting process. Therefore, understanding the performance of different catalyst for O—O bond activation is a first and fundamental step. Recently, Zhu and co-workers reported enhancement of CO oxidation by Pt decorated vacancy-abundant boron nitride nanosheet (h-BNNS) [25]. The experimental results showed the strong influence of the interfacial electronic properties for the superior catalytic activity. Therefore, the geometry and the electronic properties of interface between metal and the support plays the most crucial role in the performance of the metal catalyst. Here we have attempted to explore a novel single atom catalyst based on Co, Ni, Cu atom embedded on h-BNNS. In order to stabilize the metal atoms we have investigated the geometry and electronic structure of these elements on vacancy decorated (B- and N- vacancy) h-BN sheet. In addition, we have also investigated the nature of molecular O<sub>2</sub> interaction with embedded Co, Ni, Cu atoms with and without defects. The results are useful for understanding the stability of these metal atoms on the h-BN sheet and their performance as a catalyst for oxidative chemical reaction. Finally, as a representative case, we have also performed co-adsorption of CO and O<sub>2</sub> on Cu embedded nitrogen vacancy defected sheet and verified its potential to form CO<sub>2</sub> through oxidation.

## 2. Computational approach

A hexagonal super-cell (a, b = 15.46 Å, c = 29.6 Å) consisting of 36 boron (B) and 36 nitrogen (N) atoms has been constructed to model the pristine hexagonal BNNS (6 × 6). The spin-polarized density functional theory has been applied to calculate the total energy of all the systems studied here. The effect of van der Waals (vdW) interaction is taken into account by using the empirical correction scheme of Grimme (DFT-D2) [26]. The electron-ion interaction is described by the full-potential all-electron projector augmented wave (PAW) method, as implemented in VASP [27–30]. The generalized gradient approximation under the scheme of PBE has been used to calculate the exchange-correlation energy [31]. The cutoff energy for the plane wave basis set was fixed at 600 eV. The Brillouin Zone (BZ) of the h-BN sheet, boron vacancy defected h-BN (B<sup>V</sup>), nitrogen vacancy defected h-BN (N<sup>V</sup>), metal embedded boron vacancy (M@B<sup>V</sup>) and metal embedded nitrogen vacancy (M@N<sup>V</sup>) nano-sheet has been sampled using a Γ centered Monkhorst-Pack set of 5 × 5 × 1 K-points. The geometry optimizations have been performed by ionic relaxation, using conjugate gradient method. The geometries are considered to be converged when the forces on each ion become 0.01 eV/Å or less. In order to achieve the most optimum structure of the metal embedded h-BN nano-sheet each M atom (M = Co, Ni, Cu) is placed in and above the vacancy site of the B<sup>V</sup> and N<sup>V</sup> followed by ionic relaxation of all the atomic positions. Similar calculation is repeated further with different spin configuration to obtain the most optimum spin state of vacancy and metal embedded systems. After establishing the optimum atomic and electronic structure of the metal embedded h-BNNS, O<sub>2</sub> molecule is placed at different orientations with respect to the surface plane and close to the M atom on the B<sup>V</sup>, N<sup>V</sup>, M@B<sup>V</sup> and M@N<sup>V</sup> systems. All these systems were optimized to identify the most stable atomic configuration.

## 3. Results & discussion

To begin with we have calculated the atomic and electronic structure of the pristine and vacancy (mono) defected h-BN nano-sheet (h-BNNS, B<sup>V</sup> and N<sup>V</sup>). This is useful to further compare the changes in geometric and electronic structure of the nano-sheet after incorporation of metal atoms followed by oxygen molecule interaction using same input parameters. The optimized geometry of the pristine h-BNNS, B<sup>V</sup> and N<sup>V</sup> is

presented in Fig. S1 of the supporting information. The equilibrium bond lengths of B-N, B-B/N-N of pristine h-BNNS are 1.45 Å, 2.56 Å, respectively. The ground state structure and stability of the mono-vacancy defected h-BNNS are obtained by optimizing all atomic positions of the sheet after removal of either B or N atoms from the h-BNNS. A local distortion arises around the vacancy site after geometry optimization. The removal of one B atom creates a vacancy site (B<sup>V</sup>) surrounded by three N atoms, each having one unpaired electron in addition to one lone pair of electrons. Because of higher electron density around the vacancy site electron-electron repulsion is larger resulting these N atoms to move away from the center of the void with significant stretching of the N-N distance upto 2.82 Å. On the other hand, removal of one N atom creates a vacancy site surrounded by three B atoms (N<sup>V</sup>) each having one unpaired electron. After optimization, these B atoms reconstruct by forming an isosceles triangle with B-B distance of 2.34 and 2 × 2.61 Å. As a consequence of the above two facts, the hollow space around B<sup>V</sup> is larger than that of N<sup>V</sup>. In terms of spin polarization induced by vacancy defects, unlike pristine h-BN, both vacancy defected sheets (B<sup>V</sup> and N<sup>V</sup>) have odd electrons surrounding the defect site resulting total spin moment of 3μ<sub>B</sub> and 1μ<sub>B</sub> for B<sup>V</sup> and N<sup>V</sup>, respectively. This is in agreement with previously reported results [2,5,32]. The electronic structure and the charge distribution of these three different sheets have been analyzed via electronic density of states and charge density contours as shown in Fig. S2 and S3 in the supporting information. It is clear that the pristine h-BNNS is spin-nonpolarized and has a large energy gap between the valence and conduction band. In contrast, the B<sup>V</sup> and N<sup>V</sup> nano-sheets show odd electron states appearing in between the energy gap due to unsaturated bonds. The Fermi energy level is primarily comprised of the 2p orbital of the nitrogen. Hence the Fermi energy level of the pristine and B<sup>V</sup> are comparable but it is pushed to upwards (less negative) for the N<sup>V</sup> nano-sheet. The spin polarized nature of the B<sup>V</sup> and N<sup>V</sup> nano-sheets are clear by the difference in the electronic energy states of the up and down spin channels.

### 3.1. Interaction with single metal (M = Co, Ni, Cu) atom

Stability of isolated metal atoms on the support plays very crucial role to avoid clustering effect. While the interaction of metal atom with pristine h-BNNS is very weak, embedding the metal atom on a vacancy defect can give higher stability. For example, the energy released for Cu atom adsorption on the pristine h-BNNS is 0.6 eV and the most preferred location of Cu is at the top site of N atom with Cu-N distance of 2.16 Å. The other two sites viz. B top and hollow sites are 0.02 and 0.12 eV higher in energy, respectively. In order to verify the stability of the M atoms (Co, Ni, Cu) on the defected h-BN sheet we have optimized the geometry and electronic structure of the B<sup>V</sup> and N<sup>V</sup> after placing the metal atom “in-plane” and ‘above the plane’ at the vacancy site. Fig. 1 and Fig. S4 show the optimized structure of metal atom embedded on B<sup>V</sup> and N<sup>V</sup> systems in side and top view, respectively. In both cases the results show that the metal atom prefers to be slightly away from the plane of the sheet. In an exception to this trend, in case of Cu at the B<sup>V</sup>, the metal atom can be stabilized both in plane and out of plane locations. However, the out of plane location is more favorable. The interaction energy (E<sub>int</sub>) between the B<sup>V</sup>/N<sup>V</sup> systems and M atom is calculated as

$$E_{\text{int}} = E_{B^V/N^V}^M - E_{B^V/N^V} - E_M \quad (1)$$

where, B<sup>V</sup> or N<sup>V</sup> represents B-vacancy or N-vacancy, E<sub>B<sup>V</sup>,N<sup>V</sup></sub><sup>M</sup>, E<sub>B<sup>V</sup>,N<sup>V</sup></sub> and E<sub>M</sub> are the total energy of M@B<sup>V</sup>, M@N<sup>V</sup> systems, total energy of B<sup>V</sup>, N<sup>V</sup> system, spin polarized correction energy of the M atom. The interaction energies between M and vacancy defected sheets are listed in Table 1. It is seen that while the interaction energy of M atom (Co, Ni and Cu) with B<sup>V</sup> are -9.92, -8.85, and -6.68 eV, for interaction with N<sup>V</sup> these values are -7.25, -6.15 and -3.23 eV, respectively (negative sign indicates energy released). The large energy release by the formation of M@B<sup>V</sup>, M@N<sup>V</sup> systems clearly indicates that the metal embedded h-BN systems

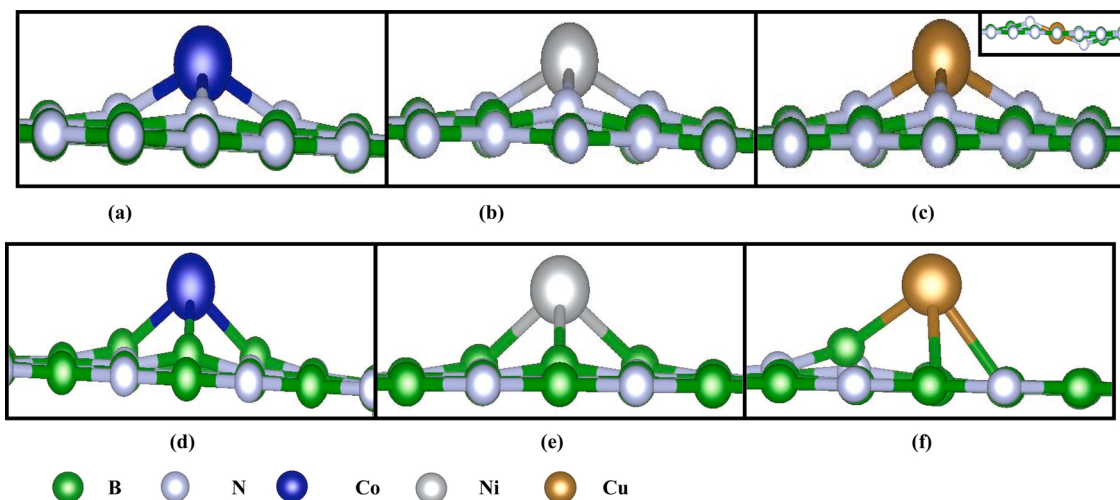


**Fig. 1.** Optimized structures of the M atom ( $M = \text{Co}, \text{Ni}, \text{Cu}$ ) on boron and nitrogen vacancy ( $M@B^V$  and  $M@N^V$ ) defected h-BN sheet. While figure a, b and c show the M atoms on boron vacancy, figure d, e and f show M atoms on nitrogen vacancy sites. The inset of the Fig. 1(c) shows the stable structure of Cu embedded  $B^V$ , where Cu atom can occupy the in-plane location.

**Table 1**

Interaction energy of metal atom with defected h-BN site (in eV), Metal-N bond length (in Å), charge on the doped M atom and height of the M atom above the h-BN plane (in Å) with  $B^V$  and  $N^V$  systems.

Properties	$\text{Co}@B^V$	$\text{Ni}@B^V$	$\text{Cu}@B^V$	$\text{Co}@N^V$	$\text{Ni}@N^V$	$\text{Cu}@N^V$
Interaction energy (eV)	-9.92	-8.85	-6.68	-7.25	-6.15	-3.23
$\text{M-N}$ bond length (Å)	1.77	1.80	1.83	1.85	1.90	1.96
$\text{B-B} / \text{N-N}$ length (at vacancy site) (Å)	2.82 (3)	2.84	2.94	2.73	2.69	2.32 2.80
Charge on M	+1.042	+1.063	+0.933	-0.084	-0.321	-0.062
Spin moment ( $\mu_B$ )	0	1.0	2.0	0	1.0	0

with boron or nitrogen vacancy are stable enough to use at room temperature.

Apart from these features the interaction energy of M atom with  $B^V$  and  $N^V$  system shows two clear patterns; (i) the interaction energy of M atom is decreasing from Co to Ni to Cu and (ii) the energy released during M atom adsorption on  $B^V$  is higher than  $N^V$  systems. Thus M atoms are more stabilized on the  $B^V$  than  $N^V$ . This is in accordance with the previous reports [33–35]. The geometrical parameters of the  $M@B^V$  and  $M@N^V$  systems are summarized in Table 1. For M embedded  $B^V$  and  $N^V$  systems, the M atom favors ‘out of plane’ locations due to the larger atomic volume of M atoms in comparison to B or N atoms. In order to underscore further insight into the nature of interaction between M and  $B^V$ ,  $N^V$  systems we have analyzed the electronic charge distribution based on Bader formalism [36]. From the charge distribution it is seen that an electronic charge of 1.042e, 1.063e, 0.933e is transferred from Co, Ni, Cu atom to  $B^V$  system, whereas 0.084e, 0.321e, 0.062e charge is transferred from  $N^V$  to Co, Ni, Cu atom, respectively. This can be explained from the large difference in the electro-negativity values of B and N atoms which are surrounding the vacancy sites.

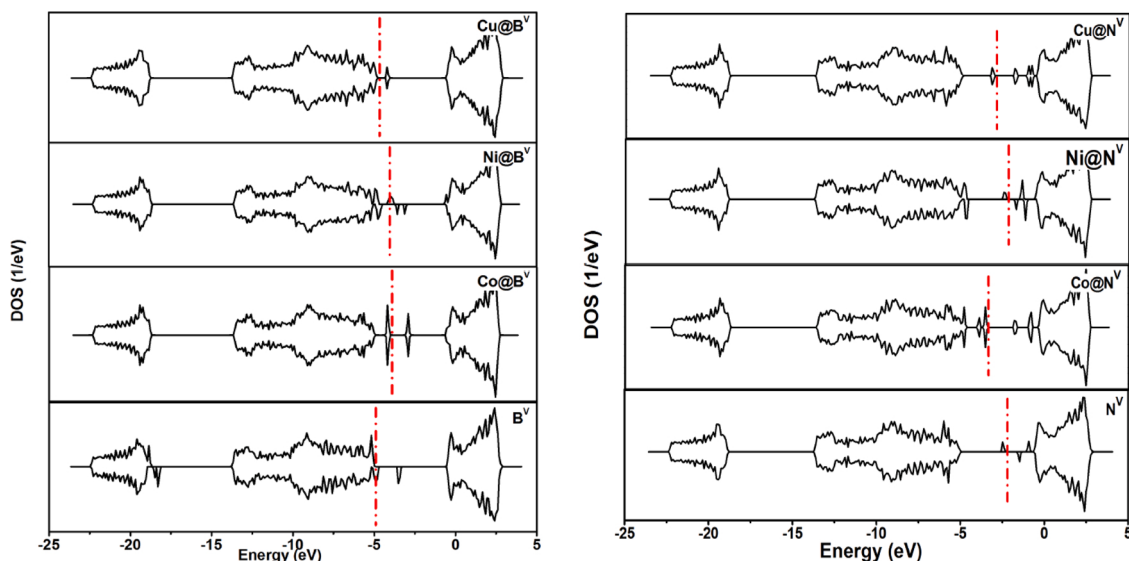


**Fig. 2.** Total density of state spectrum for  $M@B^V$  (a) and  $M@N^V$  (b) nano-sheets. For comparison, the total DOS for undoped  $B^V$  and  $N^V$  are shown in the bottom row. The Fermi energy levels are depicted by dotted lines in red color.

The nature of interaction between M and the defected sheet has been analyzed through electronic density of states (EDOS) spectrum. Fig. 2 shows the calculated density of state (DOS) spectrum of the  $M@B^V$  and  $M@N^V$  systems, respectively. In general, the incorporation of M atoms on  $B^V$  nano-sheet shifts the Fermi energy ( $E_F$ ) to higher value (less negative). For example, the  $E_F$  of the  $Co@B^V$  is shifted by 1.0 eV upwards (less negative) in comparison to  $B^V$ . From the orbital projected DOS it is seen that the Fermi energy ( $E_F$ ) level of the  $Co@B^V$  is mainly contributed by 2p orbital of the nearest N atoms of  $B^V$  and 3d orbital of the embedded Co atom. A similar trend is observed for other metals like Ni and Cu. In the case of  $Ni@B^V$  and  $Cu@B^V$  the Fermi energy levels move upwards by 0.9 eV and 0.25 eV, respectively. Thus from the chemical reactivity point of view, where electron transfer is the primary process, the  $M@B^V$  systems should show higher reactivity than undoped  $B^V$  sheet. In contrast, for  $M@N^V$  systems ( $M = Co, Cu$ ) the Fermi energy level of the  $N^V$  shifts downwards (more negative) and therefore stabilized after incorporation of the M atom. For example, the  $E_F$  of the  $Co@N^V$  and  $Cu@N^V$  shift 1.15 eV and 0.73 eV downwards, respectively. Interestingly, the  $E_F$  of  $Ni@N^V$  is remains similar to  $N^V$  system. In this context it is of interest to look into the total spin moments of the M doped  $B^V$  and  $N^V$  systems as both adsorbate and substrate possesses spin moments individually. In the gas phase, the ground state electronic configuration of the Co, Ni and Cu atoms are  $3d^74s^2$ ,  $3d^84s^2$ ,  $3d^{10}4s^1$ . As a consequence, these metal atoms show 3, 2 and 1 unpaired electrons, respectively. Upon interaction with  $B^V$ , which has three N atoms surrounding the void, the resultant spin moments for  $Co@B^V$ ,  $Ni@B^V$  and  $Cu@B^V$  become 0, 1 and 2  $\mu_B$ , respectively. Similarly for  $N^V$  system, which shows three unsaturated B atoms surrounding the vacancy site, the interaction of M atoms leads to total spin moment of 0, 1 and 0  $\mu_B$ , for  $Co@N^V$ ,  $Ni@N^V$  and  $Cu@N^V$  respectively. Because of such spin polarized electronic structure of the  $Ni@N^V$  system, the  $E_F$  level of  $Ni@N^V$  is relatively destabilized in comparison to  $Co@N^V$  and  $Cu@N^V$  systems. Moreover, the presence of M atoms not only shifts the  $E_F$  level of the  $B^V$  and  $N^V$  systems but also additional electronic states appear in the energy gap which are important to understand enhanced chemical reactivity of these systems. The charge distribution of these three sheets has been analyzed and iso-density contours are shown in Fig. S5 in the supporting information.

### 3.2. Adsorption of $O_2$ on $M$ doped $h$ -BN

It is known that for all oxidative catalysis, the activation of O—O bond plays the most vital role. Therefore, investigation of the oxygen molecule interaction with any catalyst support provides basic understanding on the feasibility of the O—O bond activation process. In this work we have explored this idea by optimizing the electronic and geometric structure of oxygen molecules interacting with all six support matrix [ $M@B^V$  and  $M@N^V$  ( $M = Co, Ni, Cu$ )]. In order to probe the activation process, we have used O—O bond length of the optimized complex ( $O_2-M@B^V$  and  $O_2-M@N^V$ ) as its change is proportional to the amount of charge transfer to the anti-bonding molecular orbital of the  $O_2$  molecule [35,37–39]. After establishing the geometric and electronic structure of isolated metal atoms with  $O_2$  molecule we have investigated the same for  $M@B^V$  and  $M@N^V$  systems. Geometrically, the  $O_2$  molecule can interact with metal embedded h-BN sheet in various orientations *viz*; (i) perpendicular, (ii) parallel and (iii) tilted with respect to the plane of the surface. In general, it is seen that in all most all cases, both  $M@B^V$  and  $M@N^V$ , the O—O bond prefers to be in parallel orientation with respect to the plane of the surface. In the following section we have described the details of the geometric and electronic structures of the oxygenated metal doped  $B^V$  and  $N^V$  systems.

#### 3.2.1. Interaction of $O_2$ with $M@B^V$

The interaction of  $O_2$  with the  $M@B^V$  ( $M = Co, Ni, Cu$ ) has been studied allowing molecular  $O_2$  towards M atom in parallel and perpendicular orientation to the h-BN sheet. The optimized structures of the  $O_2-M@B^V$  complex are shown in Fig. 3. The interaction energy of the  $M@B^V$  system with molecular  $O_2$ , charge on O atom (from Bader analysis), and O—O bond length are summarized in Table 2. It is observed that for Co embedded  $B^V$  i.e.,  $O_2-Co@B^V$ , the O—O bond prefers parallel configuration only. This means during geometry optimization, the O—O bond transformed into parallel configuration, which was initially set in perpendicular orientation. This is in line with earlier reported results [7, 18]. The interaction energy of  $O_2$  with  $Co@B^V$  system and O—O bond length after interaction are -1.31 eV and 1.35 Å, respectively. In case of  $Ni@B^V$  system, both parallel and perpendicular orientations of O—O ( $\parallel$ ,  $\perp$ ) are stable. The interaction energy of  $O_2$  with  $Ni@B^V$  system for parallel and perpendicular configurations are -1.1 eV and -0.77 eV, with

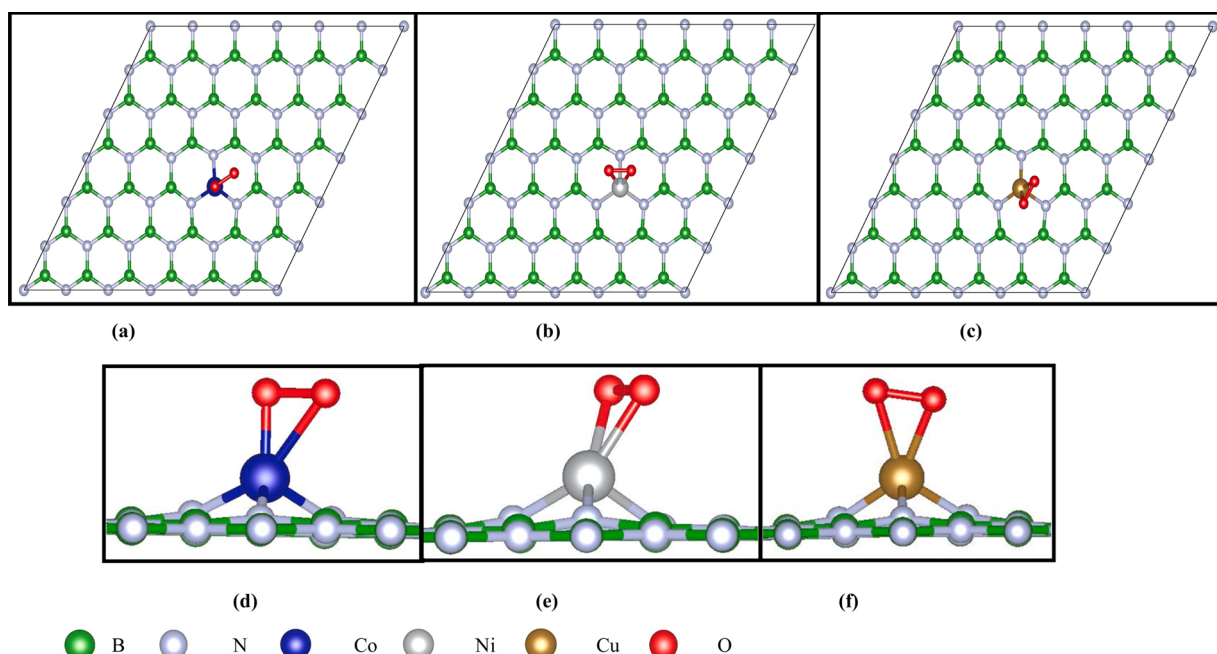


**Fig. 3.** Top and side view of the  $O_2-Co@B^V$  (a and d),  $O_2-Ni@B^V$  (b and e) and  $O_2-Cu@B^V$  (c and f) complexes.

**Table 2**

Interaction energy of  $O_2$  molecule at the metal site (in eV), Metal-O bond length ( $\text{\AA}$ ), charge on the doped M atom and O-O bond length after interaction with metal doped  $M@B^V$  and  $M@N^V$  systems.

Properties	$Co@B^V$	$Ni@B^V$	$Cu@B^V$	$Co@N^V$	$Ni@N^V$	$Cu@N^V$
<b>O-O parallel</b>						
Interaction energy (eV)	-1.31	-1.10	-0.41	-2.14	-2.68	-2.41
O-O length ( $\text{\AA}$ )	1.35	1.32	1.295	1.37	1.36	1.50
M-O length ( $\text{\AA}$ )	Co-O1 1.70 Co-O2 2.17	Ni-O1 1.95 Ni-O2 1.95	Cu-O1 1.97 Cu-O2 2.09	Co-O1 1.85 Co-O2 1.91	Ni-O1 1.93 Ni-O2 1.93	Cu-O1 1.83 Cu-O2 1.85
Charge on $O_2$	-0.62	-0.45	-0.33	-0.64	-0.65	-1.0
Spin moment ( $\mu_B$ )	0	1.0	0	2.0	1.0	0
<b>O-O perpendicular</b>						
Interaction energy (eV)		-0.77	-0.29			-1.06
O-O length ( $\text{\AA}$ )		1.28	1.26			1.35
M-O		Ni-O1 1.77 Ni-O2 2.74	Cu-O1 1.80 Cu-O2 2.82			Cu-O1 1.90 Cu-O2 2.83
Charge on $O_2$	-	-0.30	-0.19			-0.384
Spin moment ( $\mu_B$ )	-	1.0	0			0

$O-O$  bond elongated upto 1.32 and 1.28  $\text{\AA}$ , respectively. Similarly, for the interaction of  $O_2$  with  $Cu@B^V$ , both parallel and perpendicular orientations are stable with interaction energy of -0.41 and -0.29 eV, respectively. The weak interaction leads to marginal increase in  $O-O$  bond upto 1.29  $\text{\AA}$ . The total spin moment of the  $O_2\text{-Co}@B^V$ ,  $O_2\text{-Ni}@B^V$  and  $O_2\text{-Cu}@B^V$  complexes are 0, 1, and 0  $\mu_B$ , respectively.

The electronic structure of the  $M@B^V$  with  $O_2$  has been analyzed through electronic density of states spectrum as shown in Fig. 4. It is seen that after  $O_2$  interaction the Fermi energy levels are more stabilized as compared to the  $M@B^V$ . The trend in the  $E_f$  values suggest more electronic stability as we move from  $O_2||Co@B^V$  (-4.42 eV) to  $O_2||Ni@B^V$  (-4.64 eV) to  $O_2||Cu@B^V$  (-4.72 eV) system. From the Bader charge analysis it is seen that an electronic charge of 0.62e, 0.45e and 0.33e are transferred from  $Co@B^V$ ,  $Ni@B^V$  and  $Cu@B^V$  system to the anti bonding orbital of the oxygen molecule (parallel configuration). Further we note that in case of perpendicular orientation of  $O-O$  bond, the charge transfer is relatively less. These results clearly indicate the difference in spatial orbital overlap between parallel (bi-dented) and perpendicular (mono-dented) configurations of  $O_2$  and M atoms. An ‘in-depth’ Bader charge distribution is also carried out for the M and neighboring ‘in plane’ N atoms for all systems. The effect of  $O_2$  on the electronic properties of  $M@B^V$  has also been examined by plotting the projected density of states (PDOS) of the  $O_2||M@B^V$  systems. The PDOS spectrum of O and M atom in  $O_2||M@B^V$  systems are shown in Fig. S6. It is seen that there is significant overlap between 2p orbital of O and 3d orbital of the respective M atoms at the Fermi energy level. Moreover, the  $E_f$  values of  $O_2||M@B^V$  systems are more negative than  $M@B^V$  systems of the respective M atoms. This change of the  $E_f$  in Cu system is much smaller than that for other systems with Co and Ni. This is because of lower electronic charge transfer from  $Cu@B^V$  to the anitibonding orbital of the oxygen molecule.

### 3.2.2. Interaction of $O_2$ with $M@N^V$

Unlike the  $B^V$  sheet, where the vacancy site is surrounded by three electronegative nitrogen atoms, the nitrogen vacancy site is surrounded by three relatively lesser electronegative boron atoms. As a consequence, it is more likely that the embedded M atoms at the vacancy site will have more free electrons to bind with other system. Here we have investigated the interaction of  $O_2$  molecules with  $M@N^V$  ( $M = Co, Ni, Cu$ ) systems. For optimization, we have used the same approach as mentioned in case of  $M@B^V$  systems. The optimized structures of the  $O_2\text{-}M@N^V$  complexes are shown in Fig. 5. Some of the salient features are; (i) the interaction energy between  $M@N^V$  and  $O_2$  molecules are higher (in the range of 2.14–2.68 eV) as compared to the  $M@B^V$  systems, (ii) for  $Ni@N^V$  and  $Co@N^V$ , the  $O-O$  bond lengths are 1.36 and 1.37  $\text{\AA}$ , respectively and for  $Cu@N^V$ , the  $O-O$  bond length elongates upto 1.50  $\text{\AA}$ . The longer  $O-O$  bond lengths are consequence of higher charge transfer from the M to the anti-bonding orbital of the  $O_2$  molecule. It should be mentioned here that for oxygen molecule, the  $O-O$  bond activation leads to two different oxidation states of  $O_2$ . While in the super-oxo state the  $O-O$  bond elongates in the range of 1.32–1.36  $\text{\AA}$ , for the per-oxo state the  $O-O$  bond elongates upto 1.50  $\text{\AA}$ . The total spin moment of the  $O_2\text{-Co}@N^V$ ,  $O_2\text{-Ni}@N^V$  and  $O_2\text{-Cu}@N^V$  are 2, 1, and 0  $\mu_B$ , respectively.

The electronic structure of the  $M@N^V$  with  $O_2$  has been analyzed through electronic density of states spectrum as shown in Fig. 6. It is seen that after  $O_2$  interaction the Fermi energy levels are more stabilized as compared to the  $M@N^V$ . The trend in the  $E_f$  values suggest more electronic stability as we move from  $O_2||Co@B^V$  (-3.82 eV) to  $O_2||Ni@B^V$  (-3.77 eV) to  $O_2||Cu@B^V$  (-2.42 eV) system. From the Bader charge analysis it is seen that an electronic charge of 0.64e, 0.65e and 1.0e have been transferred from  $Co@N^V$ ,  $Ni@N^V$  and  $Cu@N^V$  system to the anti bonding orbital of the oxygen molecule (parallel configuration). The amount of charge transfer is relatively higher in  $M@N^V$  systems that that

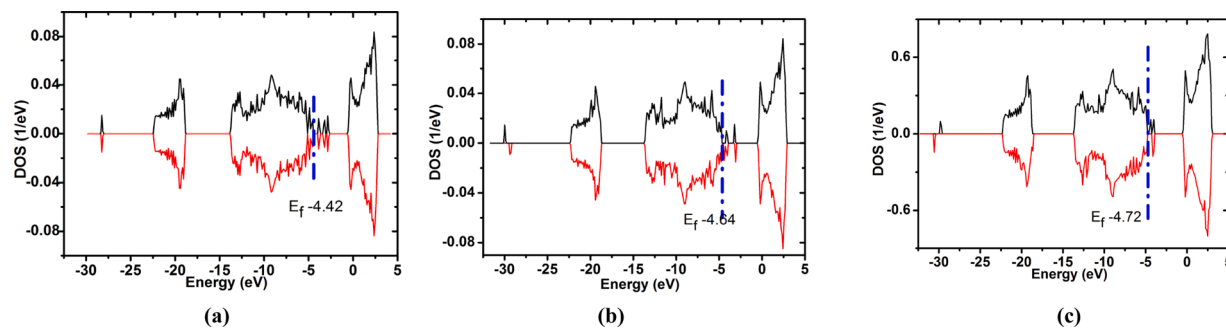
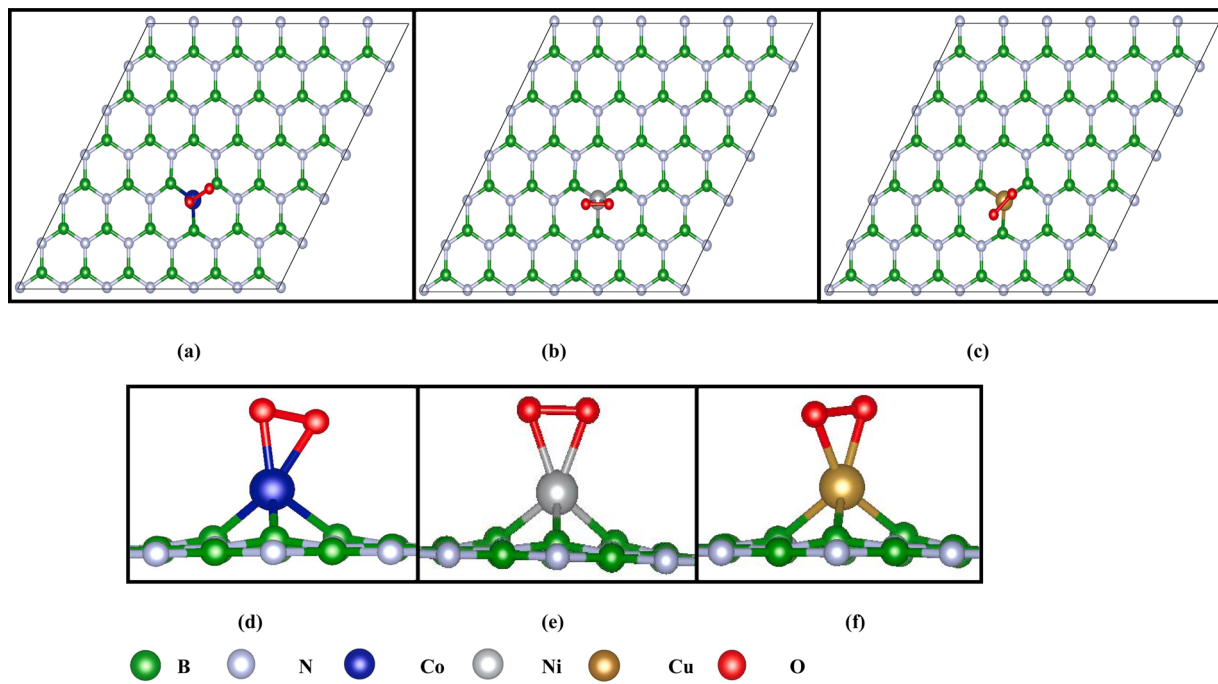
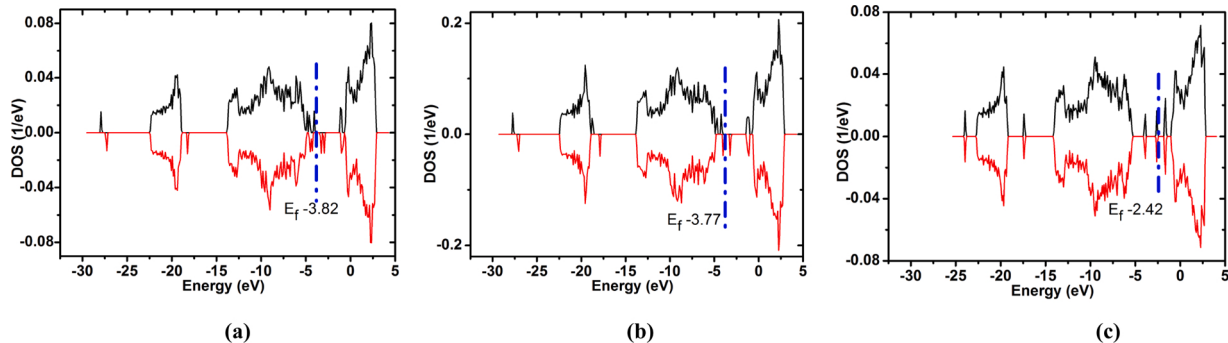


Fig. 4. The total density of states of (a)  $O_2\text{-Co}@B^V$  system (b)  $O_2\text{-Ni}@B^V$  system and (c)  $O_2\text{-Cu}@B^V$  system. (The Fermi level is indicated by dotted vertical line).



**Fig. 5.** Top and side view of the  $O_2$ -Co@ $N^V$  (a and d),  $O_2$ -Ni@ $N^V$  (b and e) and  $O_2$ -Cu@ $N^V$  (c and f) complexes.



**Fig. 6.** The total density of states of (a)  $O_2$ -Co@ $N^V$  system (b)  $O_2$ -Ni@ $N^V$  system and (c)  $O_2$ -Cu@ $N^V$  system. (The Fermi level is indicated by dotted vertical line).

of M@ $B^V$  systems. This explains the higher O—O bond length (per-oxo state) in  $O_2||M@N^V$  system in comparison to O—O bond length (super-oxo state) in  $O_2||M@B^V$  system. The site projected density of states analysis of O and M atom in  $O_2||M@N^V$  systems are represented in Fig. S7. The charge distribution of these sheets ( $O_2||M@B^V$  and  $O_2||M@N^V$  systems) have been analyzed and the iso-density contours are shown in Fig. S8. It is seen that there is significant overlap between 2p orbital of O and 3d orbital of the respective M atom, responsible for longer O—O bond. Interestingly, the contribution of 2p orbital of  $O_2$  in  $O_2$ -Cu@ $N^V$  is relatively higher than that of 2p orbital's of O in other systems (M = Co, Ni). This further corroborates the larger stretching of O—O bond for Cu@ $N^V$  nano-sheet.

In order to verify the performance of these single atom catalysts we have performed a case study for CO oxidation on the Cu@ $N^V$  system. It is seen that unlike  $O_2$ , the CO preferred to adsorb in perpendicular way and the adsorption energy is calculated to be -1.46 eV. In the next step we have co-adsorb both CO and  $O_2$  on the Cu@ $N^V$ . After optimization, the O—O bond ruptures and one of the oxygen atoms binds with CO to form  $CO_2$  and thereafter  $CO_2$  desorbs from the Cu@ $N^V$  sheet (Fig. 7). This clearly demonstrates the efficiency of this catalyst for oxidation reactions.

#### 4. Conclusion

The O—O bond activation by metal atom (Co, Ni and Cu) embedded h-BN sheet (with B or N vacancy) has been investigated using the density functional theory. Through this work we have explored the feasibility of stabilizing a metal atom on vacancy defected h-BN sheet and the nature of interaction of the embedded single metal atom with  $O_2$  molecule. The geometric and electronic structure optimizations have been carried out to obtain the ground state atomic configuration and electronic structure. The interaction of molecular oxygen with the metal atoms embedded on the h-BNNS has been investigated by placing the oxygen molecule at different orientations with respect to the plane. The results have been analyzed by the binding energy, geometrical parameters, charge distribution and the electronic density of state analysis. The results revealed higher stability of metal atoms on the vacancy defects in comparison to the pristine surface. Moreover, the stability of metal atoms is more on the B vacancy defect than N vacancy. Bader charge analysis showed that with M atoms on B vacancy, the BNNS acts as a Lewis acid by accepting electrons. In sharp contrast, for M atoms on N vacancy, the BNNS acts as Lewis base by donating charge to the metal centers. The electronic density of state analysis suggests the upward move (less negative) of the Fermi energy levels due to incorporation of M atoms. From the chemical reactivity point of view embedded metal atoms promote (in comparison

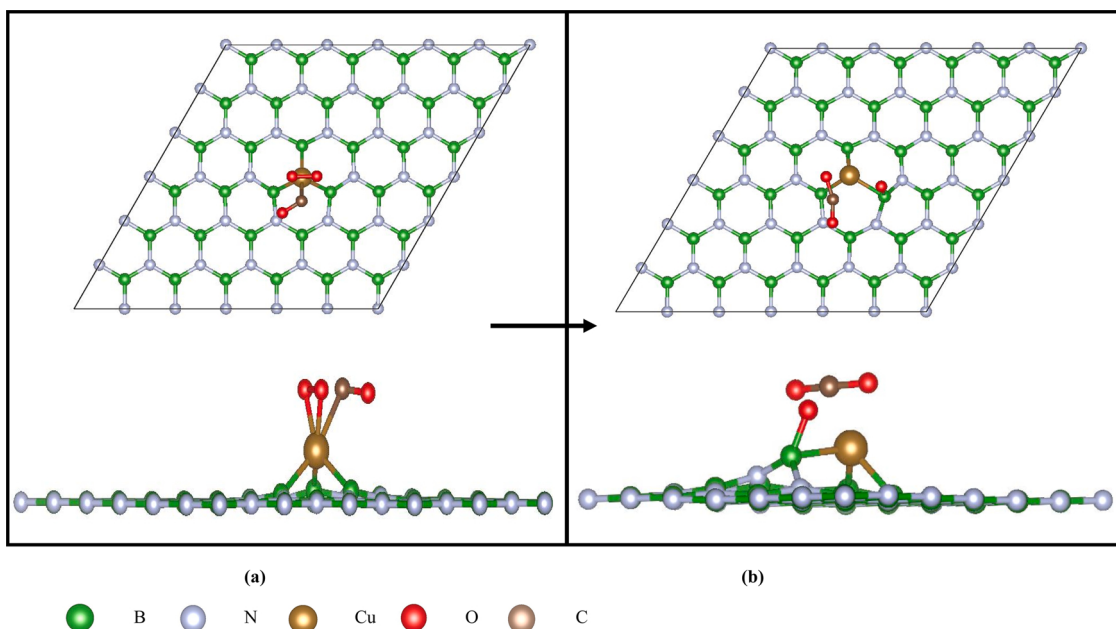


**Fig. 7.** Initial and final geometries (top and side view are shown in the upper and lower panel) of the CO and O<sub>2</sub> co-adsorption on the Cu@N<sup>V</sup> nano-sheet.

to bare metal atoms) the electronic charge transfer to the anti-bonding molecular orbital of the O<sub>2</sub> molecule.

The activation of the O—O bond has been illustrated through the change in the bond length, which is proportional to the charge transfer from the metal to the anti-bonding orbitals of the O<sub>2</sub> molecule. The results show that the M atom embedded N vacancy defects elongate the O—O bond more than M atoms on B vacancy defects. Because of weaker interaction of metal atoms with N vacancy sites they have more free electrons and thereby are able to activate the O—O bond more efficiently. In fact the most stable isomer of O<sub>2</sub> with Cu@N<sup>V</sup>, the O—O bond can be stretched upto 1.50 Å (which is considered as the peroxy state of the O<sub>2</sub> molecule) for Cu embedded in the N vacancy site of the h-BN. In order to verify the efficiency of these systems we have performed CO oxidation on Cu@N<sup>V</sup> as a case study. The results demonstrated spontaneous formation of the CO<sub>2</sub> molecule for CO and O<sub>2</sub> co-adsorption. On the basis of these results it is inferred that metal atom embedded nitrogen vacancy defects are more efficient for O—O bond activation.

#### Declaration of Competing Interest

The authors declare that they have no known competing financial interests or personal relationships that could have appeared to influence the work reported in this paper.

#### Acknowledgments

The authors acknowledge all staff members of the Computer Division of VECC, Kolkata for providing supercomputing facility. J. Datta thanks Head, Analytical Chemistry Division, and Associate Director, Chemistry Group for the necessary permission and support.

#### Appendix A. Supplementary data

Supplementary material related to this article can be found, in the online version, at doi:<https://doi.org/10.1016/j.cattod.2020.10.021>.

#### References

- [1] A.H. Wasey, S. Chakrabarty, G.P. Das, C. Majumder, h-BN Monolayer on the Ni (111) surface: a potential catalyst for oxidation, *ACS Appl. Mater. Interfaces* 5 (21) (2013) 10404–10408.
- [2] B. Huang, H. Lee, Defect and impurity properties of hexagonal boron nitride: a first-principles calculation, *Phys. Rev. B* 86 (2012), 245406.
- [3] C. Attaccalite, M. Bockstedte, A. Marini, A. Rubio, L. Wirtz, Coupling of excitons and defect states in boron-nitride nanostructures, *Phys. Rev. B* 83 (2011), 144115.
- [4] M. Topsakal, E. Aktürk, S. Ciraci, First-principles study of two- and one-dimensional honeycomb structures of boron nitride, *Phys. Rev. B* 79 (2009), 115442.
- [5] M. Si, D.S. Xue, Magnetic properties of vacancies in a graphitic boron nitride sheet by first-principles pseudopotential calculations, *Phys. Rev. B* 75 (2007), 193409.
- [6] S. Back, S. Siahostami, Noble metal supported hexagonal boron nitride for the oxygen reduction reaction: a DFT study, *Nanoscale Adv.* 1 (2019) 132–139.
- [7] C. Deng, R. He, W. Shen, M. Li, T. Zhang, Single-atom catalyst of cobalt supported on a defective two-dimensional boron nitride material as a promising electrocatalyst for the oxygen reduction reaction: a DFT study, *Phys. Chem. Chem. Phys.* 21 (2019) 6900–6907.
- [8] S. Lin, X. Ye, R. Johnson, H. Guo, First-principles investigations of metal (Cu, Ag, Au, Pt, Rh, Pd, Fe, Co, and Ir) doped hexagonal boron nitride nanosheets: stability and catalysis of CO Oxidation, *J. Phys. Chem. C* 117 (33) (2013) 17319–17326.
- [9] Q. Liu, Z. Zhang, Platinum single-atom catalysts: a comparative review towards effective characterizations, *Catal. Sci. Technol.* 9 (2019) 4821–4834.
- [10] N. Cheng, L. Zhang, K. Doyle-Davis, X. Sun, Single-atom catalysts: from design to applications, *Electrochim. Energ.* 2 (2019) 539–573.
- [11] L. Zhang, H. Liu, S. Liu, M. Norouzi Banis, Z. Song, J. Li, et al., Pt/Pd single-atom alloys as highly active electrochemical catalysts and the origin of enhanced activity, *ACS Catal.* 9 (2019) 9350–9358.
- [12] C. Rivera-Cárcamo, P. Serp, Single-atom catalysts on carbon-based materials, *Chem. Cat. Chem.* 10 (2018) 5058.
- [13] G.R. Bhimanapati, Z. Lin, V. Meunier, Y. Jung, J. Cha, S. Das, et al., Recent advances in two-dimensional materials beyond graphene, *ACS Nano* 9 (2015) 11509–11539.
- [14] Y. Lin, C.E. Bunker, K.A. Fernando, J.W. Connell, Aqueously dispersed silver nanoparticle-decorated boron nitride nanosheets for reusable, thermal oxidation-resistant surface enhanced Raman spectroscopy (SERS) devices, *ACS Appl. Mater. Interfaces* 4 (2012) 1110–1117.
- [15] A. Nagashima, N. Tejima, Y. Gamou, T. Kawai, C. Oshima, Electronic dispersion relations of monolayer hexagonal boron nitride formed on the Ni(111) surface, *Phys. Rev. B* 51 (7) (1995) 4606–4613.
- [16] W. Auwärter, M. Muntwiler, T. Greber, J. Osterwalder, Co on h-BN/Ni(111): from island to island-chain formation and Co intercalation, *Surf. Sci.* 511 (2002) 379–386.
- [17] X. Liu, T. Duan, Y. Sui, C. Meng, Y. Han, Copper atoms embedded in hexagonal boron nitride as potential catalysts for CO oxidation: a first-principles investigation, *RSC Adv.* 4 (2014) 38750–38760.
- [18] Z. Liu, P. Lv, Y. Liang, D. Ma, Y. Zhang, W. Zhang, et al., CO oxidation catalyzed by the single Co atom embedded hexagonal boron nitride nanosheet: a DFT-D study, *Phys. Chem. Chem. Phys.* 18 (2016) 21865–21870.
- [19] Y. Liu, L. Yang, E. Ganz, First-principles investigations of single metal atoms (Sc, Ti, V, Cr, Mn, and Ni) embedded in hexagonal boron nitride nanosheets for the catalysis of CO Oxidation, *Cond. Matt.* 4 (2019) 65.
- [20] W. Sun, Y. Meng, Q. Fu, F. Wang, G. Wang, W. Gao, et al., High-yield production of boron nitride nanosheets and its uses as a catalyst support for hydrogenation of nitroaromatics, *ACS Appl. Mater. Interfaces* 8 (15) (2016) 9881–9888.

- [21] R. Zhang, X. Yang, Z. Tao, X. Yang, H. Yang, L. Yang, et al., Insight into the effective aerobic oxidative cross-esterification of alcohols over Au/porous boron nitride catalyst, *ACS Appl. Mater. Interfaces* 11 (50) (2019) 46678–46687.
- [22] Z. Ma, Z. Cui, C. Xiao, W. Dai, Y. Lv, Q. Li, et al., Theoretical screening of efficient single-atom catalysts for nitrogen fixation based on a defective BN monolayer, *Nanoscale* 12 (2020) 1541–1550.
- [23] A.H.M. Wasey, G.P. Das, C. Majumder, Exploring the effect of oxygen coverage on the electronic, magnetic and chemical properties of Ni(111) supported h-BN sheet: a density functional study, *Chem. Phys. Lett.* 676 (2017) 124–128.
- [24] X. Gao, S. Wang, S. Lin, Defective hexagonal boron nitride nanosheet on Ni(111) and Cu(111) stability, electronic structures, and potential applications, *ACS Appl. Mater. Interfaces* 8 (2016) 24238–24247.
- [25] W. Zhu, Z. Wu, G. Foo, X. Gao, M. Zhou, B. Liu, et al., Taming interfacial electronic properties of platinum nanoparticles on vacancy-abundant boron nitride nanosheets for enhanced catalysis, *Nat. Commun.* 8 (2017) 15291.
- [26] S. Grimme, Semiempirical GGA-Type Density functional constructed with a long-range dispersion correction, *J. Comput. Chem.* 27 (2006) 1787–1799.
- [27] P.E. Blochl, Projector augmented-wave method, *Phys. Rev. B* 50 (1994) 17953–17979.
- [28] G. Kresse, J. Furthmüller, Efficiency of *ab initio* total energy calculations for metals and semiconductors using a plane-wave basis set, *Comput. Mater. Sci.* 6 (1) (1996) 15–50.
- [29] G. Kresse, J. Hafner, Ab initio molecular-dynamics simulation of the liquid-metal–amorphous–semiconductor transition in germanium, *Phys. Rev. B* 49 (1994) 14251–25269.
- [30] G. Kresse, D. Joubert, From ultrasoft pseudopotentials to the projector augmented-wave method, *Phys. Rev. B* 59 (1999) 1758–1775.
- [31] J.P. Perdew, K. Burke, M. Ernzerhof, Generalized gradient approximation made simple, *Phys. Rev. Lett.* 77 (1996) 3865–3868.
- [32] S. Banerjee, C. Majumder, Stability and electronic properties of Au atom doped hexagonal boron nitride sheet on Ni(111) support: role of vacancy defects and supports towards single atom catalysis, *Appl. Surf. Sci.* 515 (2020), 145978.
- [33] C. Jin, F. Lin, K. Suenaga, S. Iijima, Fabrication of a freestanding boron nitride single layer and its defect assignments, *Phys. Rev. Lett.* 102 (2009), 195505.
- [34] A. Du, Y. Chen, Z.H. Zhu, R. Amal, G.Q. Lu, S.C. Smith, Dots versus antidots: computational exploration of structure, magnetism, and half-metallicity in boron–nitride nanostructures, *J. Am. Chem. Soc.* 131 (2009) 17354–17359.
- [35] M. Gao, A. Lyalin, T. Taketsugu, Catalytic activity of Au and Au<sub>2</sub> on the h-BN surface: adsorption and activation of O<sub>2</sub>, *J. Phys. Chem. C* 116 (16) (2012) 9054–9062.
- [36] R.F.W. Bader, Atoms in molecules, *Acc. Chem. Res.* 18 (1985) 9–15.
- [37] J. Huang, S. He, J.L. Goodsell, J.R. Mulcahy, W. Guo, A. Angerhofer, et al., Manipulating atomic structures at the Au/TiO<sub>2</sub> interface for O<sub>2</sub> activation, *J. Am. Chem. Soc.* 142 (2020) 6456–6460.
- [38] N. Siemer, A. Lüken, M. Zalibera, J. Frenzel, D. Muñoz-Santiburcio, A. Savitsky, et al., Atomic-scale explanation of O<sub>2</sub> activation at the Au–TiO<sub>2</sub> interface, *J. Am. Chem. Soc.* 140 (2018) 18082–18092.
- [39] G.L. Gutsev, B.K. Rao, P. Jena, Systematic study of oxo, peroxy, and superoxo isomers of 3d-metal dioxides and their anions, *J. Phys. Chem. A* 104 (2000) 11961–11971.